Surface reconstruction by means of a flexible sensor array

Eugen Koch, Andreas Dietzel, TU Braunschweig Institut für Mikrotechnik, Alte Salzdahlumer Str. 203, 38124 Braunschweig, Deutschland, eugen.koch@tu-bs.de

Abstract

In recent years, an increasing popularity of flexible sensor systems has been observed, which can largely be attributed to their ability to continuously adapt the shape to deformable bodies with non-planar surfaces without losing functionality. In this paper, we present a self-sensing, ultra-thin and flexible sensor array foil, which allows for determining its actual shape by analyzing signals from 6x6 sensors. Raw sensor signals clearly show the dependence from strength and direction of bending. The local bending vector is determined from signals of sensors oriented in different directions using rules which are already applied for strain gauge rosettes. The algorithm for the surface reconstruction divides the sensor foil into discrete bending segments for which the bending and subsequently new coordinates of segment edges are determined. A sensor diagnostics routine intercepts failure of the complete system due to the failure of single sensors. The functionality of the sensor array and the surface reconstruction is demonstrated for a foil subsequently adapting to a tube in different orientations. The obtained surface reconstruction clearly correlates with the visually observed bending. Such surface reconstruction could provide diagnostic information and potentially be used to detect diseases like pneumothorax. It could not only help to improve medical treatments but also to monitor the structural health of technical constructions.

Keywords: surface reconstruction, topography capturing, flexible systems, systems-in-foil, sensor array, curvature sensing

1 Introduction

In recent years, there has been growing interest in capturing the surface topography of deformable objects and exploiting this information to establish a variety of new smart systems. This trend has led to the development of topography capturing devices, which can be categorized as: *self-sensing* devices in which sensors are embedded into a deforming surface to directly measure local deformations and *external-sensing* devices, which require external sensing equipment like projectors and cameras to capture the surface deformations [1]. Microsoft Kinect [2] is probably the most famous vision-based *external-sensing* device for surface reconstruction. Such systems show very good surface reconstruction results but they require an undistorted field of view, which will suffer from any occlusions limiting their use in mobile applications. This paper focuses on *self-sensing* devices which can be distinguished on the basis of the employed shape sensing techniques. A simple device like Bookisheet [3] for example uses just two bending sensors to categorize discrete bend gestures which are used to flip through pages of an e-book. FlexRemote [4] uses 16 sensors and recognizes eight bend gestures to control a television. These systems are not aiming for accurate surface reconstruction. Other systems like ShapeTape [5], which is a long rubber tape with integrated fiber optic bend sensors and SensorTape [6], which is a long polyester tape with integrated accelerometer and gyroscope sensor chips are able to detect 3D bending and twisting of curved shapes. Such systems could be used as graphical input devices, for example by a CAD designer to easily enter arbitrary shapes into CAD software [5], or as a digital ruler to measure the shape of 3D objects [6]. A further promising application of such systems could be the measurement of deformations of a human backbone by attaching a flexible sensor tape directly to the skin [6,7] or integrating it into the clothing. Because many people suffer from backache due to incorrect posture, such kind of device could directly alert people when their posture worsens. It could subsequently analyze collected data to identify impairing physical activities, and hence increase the user's consciousness of healthy body movement. In the fast growing sector of virtual reality, applying such devices to the joints of the human body could become a very attractive technique for measuring body movements and controlling virtual reality applications in a similar fashion as with already existing data gloves [8]. For a more complex 2.5D surface

https://doi.org/10.24355/dbbs.084-201904011542-0

reconstruction, FlexSense [1] uses 16 printed piezoelectric sensors on a thin, transparent A4-size plastic substrate. A pre-processing training phase on the basis of vision-based 3D ground truth measurements is used to infer the shape of the foil by either linear interpolation or a more sophisticated machine learning approach. Possible applications of such shape sensing systems could be, for example, using them as deformable input/output (IO) devices for digital interaction, in particular gaming [1].

In previous work, we have developed a thin sensor foil with strain gauge based bending sensors in a Wheatstone bridge configuration which provides voltage output proportional to the local bending without signal decay, as is typical for piezoelectric sensors and hence does not suffer from the related sensor drift [9]. A detailed description of the fabrication process and the characteristics of obtained signals has already been provided earlier[9] . Instead of long tape-like sensors [5,6] or relatively large sized (A4) plastic substrates [1] we developed a rather small ultra-thin, flat polyimide foil with a relatively high sensor density which could be exploited in applications focusing on smaller surface dimensions. This paper describes a newly developed method and algorithm to reconstruct the surface of this self-sensing flexible sensor array foil on the basis of bending measurements at 36 separate points.

2 Sensor design & operation

This chapter gives a brief overview of the sensor design, the operation principle, and the sensor array architecture as necessary to understand the surface reconstruction approach. **Figure 1a** shows a bended flexible sensor array consisting of 6x6=36 single sensor elements with alternating orientations in four different directions ($s_0, s_{45}, s_{90}, s_{135}$), as indicated in **Figure 1b.** Each sensor element itself consists of four metal strain gauges in a configuration illustrated by the 3D-CAD drawing in **Figure 1c.** The appropriate electrical connection to a full Wheatstone bridge is shown in **Figure 1d**. To achieve a better sensitivity we designed so called "double-sided" sensor elements by placing two resistors on the top side (R2, R3) and the two others (R1, R4) on the bottom side of the foil substrate.

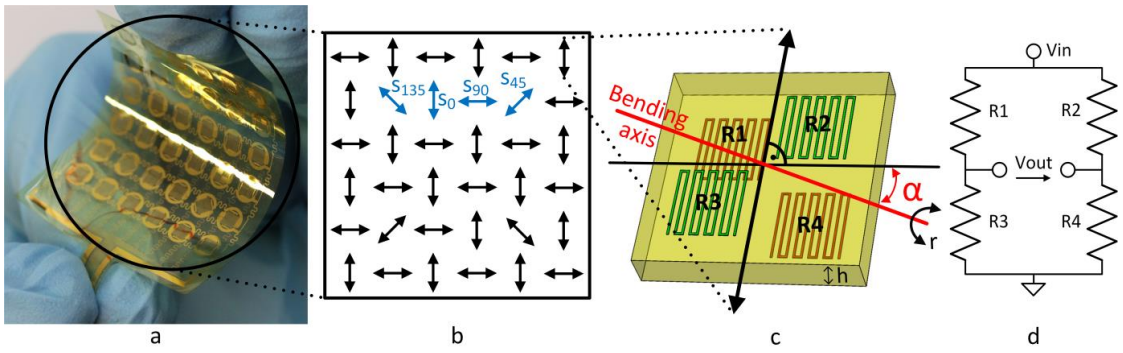

Figure 1: (a) Hand-bended 6x6 sensor array, (b) illustration and definition of sensor orientations ($s_0, s_{45}, s_{90}, s_{135}$), within the 6x6 array structure, (c) illustration of the double-sided sensor design, (d) schematic illustration of implemented full Wheatstone bridge configuration.

Bending of the sensor foil over an axis with the bending radius r and the orientation angle α according to **Figure 1c** would lead to an elongation of resistors on one surface and to a compression of the resistors on the opposite surface. This bending leads to an output signal $V_{out}(\alpha, r)$, which is a function of the bending radius r and the bending orientation angle α but also depends on the Wheatstone bridge supply voltage V_{in} (in our case 3.3 V) and the interlayer thickness h (in our case 11.5 µm) between top and bottom sensor layers. For purely longitudinal deformation of the resistors ($\alpha = 0°$) we achieved output signals as:

$$V_{out}(0°, r) = V_{in} \cdot \frac{h}{r} \tag{1}$$

For bending orientations at $\alpha \neq 0°$ a reduced signal $V_{out}(\alpha, r)$ is obtained as:

https://doi.org/10.24355/dbbs.084-201904011542-0

$$V_{out}(\alpha, r) = V_{out}(0°, r) \cdot \left[\frac{(1+q)}{2} + \frac{(1-q)}{2} \cdot \cos(2\alpha)\right] \quad (2)$$

Factor q represents the transversal sensitivity of a strain gauge, which for our sensor was experimentally determined to be q=0.3 (+/-0,05). This relation, which is equivalent to one applied for conventional strain gauge rosettes for determining the three components of an in-plain strain [10], is plotted in **Figure 2**. Measurements obtained with two different sensors are in good agreement with **Eq. (2).**

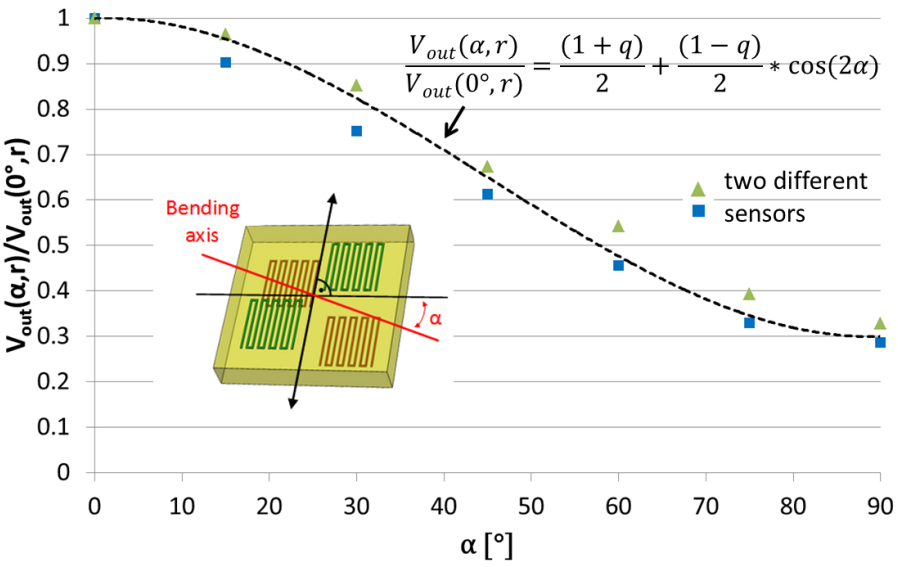

Figure 2: Diagram showing the sensor output reduction $\frac{V_{out}(\alpha,r)}{V_{out}(0°,r)}$ as function of bending orientation angle α. The dashed line represents Eq. 2, whereas the data points are experimentally obtained from two different sensors

With the aid of the signals from three sensors in different orientations V_{s0}, V_{s45}, V_{s90}, the bending angle α can be determined unambiguously as follows [10]:

(1) If $V_{s90} < V_{s0}$ -> $\alpha = \frac{1}{2} tan^{-1}\left(\frac{2 \cdot V_{s45} - V_{s90} - V_{s0}}{V_{90} - V_0}\right)$

(2) If $V_{s90} > V_{s0}$ -> $\alpha = \frac{1}{2} tan^{-1}\left(\frac{2 \cdot V_{s45} - V_{s90} - V_{s0}}{V_{s90} - V_{s0}}\right) + 90°$

(3) If $V_{s90} = V_{s0}$ and $V_{s45} < V_{s90}$ -> $\alpha = -45°$

(4) If $V_{s90} = V_{s0}$ and $V_{s45} > V_{s90}$ -> $\alpha = +45°$

Figure 3 illustrates the sensor array response by bending the foil in an S-shape **(left)**. The dependence between sensor orientation and signal amplitudes, as well as the change of bending polarity by the switch of the signal sign from positive to negative values can be seen **(right)**.

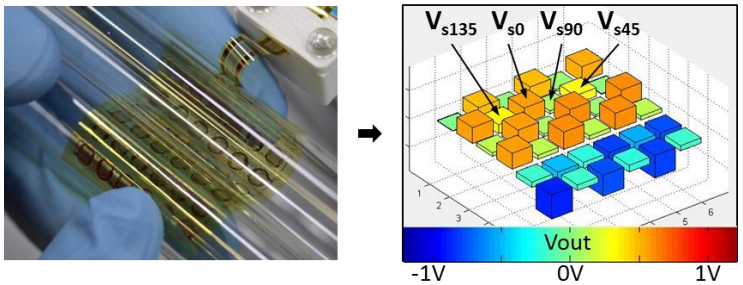

Figure 3: Illustration of sensor operation: S-shape bending (left), resulting raw sensor signals in a bar chart presentation (right)

https://doi.org/10.24355/dbbs.084-201904011542-0

Sensor signals are processed using home-built electronics, shown in **Figure 4,** consisting of two main parts; a multiplexing PCB and a controller PCB which are connected via HDMI.

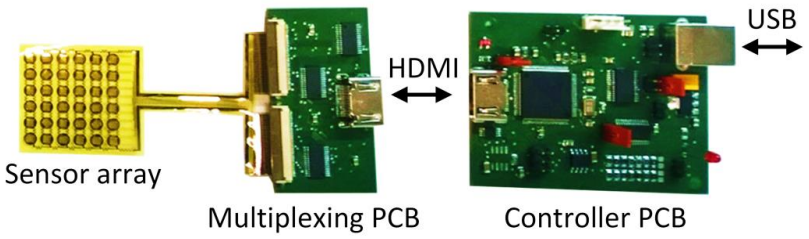

Figure 4: Sensor array with evaluation electronics

The multiplexing PCB is directly connected to the sensor array and converts the incoming 72 analog sensor signals to only 2 analog signals for the controller PCB, where the signal is processed (offset compensation, amplification, low-pass filtering, digitalization) and subsequently sent to a PC via USB connection for the final data processing and visualization using MATLAB software.

3 Principle of surface reconstruction

All 36 sensors $S_{ij}(x_{ij}, y_{ij}, z_{ij})$, $(i = 1 \dots 6\,; j = 1 \dots 6)$ are placed in a 3D Cartesian coordinate system. Initially (before bending), all sensors are located in the z=0 plane, evenly spaced with a distance of 1 and the coordinates $S_{ij}(i - 3.5, 3.5 - j, 0)$, as seen in **Figure 5.**

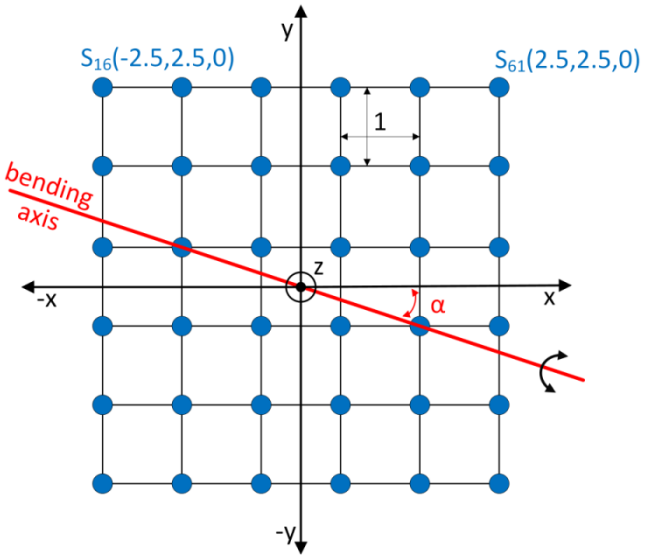

Figure 5: Arrangement of sensors $S_{ij}\left(x_{ij}, y_{ij}, z_{ij}\right)$, in a 3D Cartesian coordinate system with the definition of bending axis and bending orientation angle α relative to the sensor array.

The reconstruction algorithm is simplified by permitting only one bending axis for the complete sensor array, which reflects the fact that the sensor foil is bendable but not stretchable. The anchor point for the bending axis is the origin of the coordinate system (see **Figure 5)**. The bending axis divides the sensor array in two halves for which the surface reconstruction is analogous.

With the knowledge of bending angle α we are able to divide the sensor array in to discrete bending segments with the length $l_{(n)}$, $(n = 1 \dots N\ with\ 6 \leq N \leq 36)$, as shown in **Figure 6**.

https://doi.org/10.24355/dbbs.084-201904011542-0

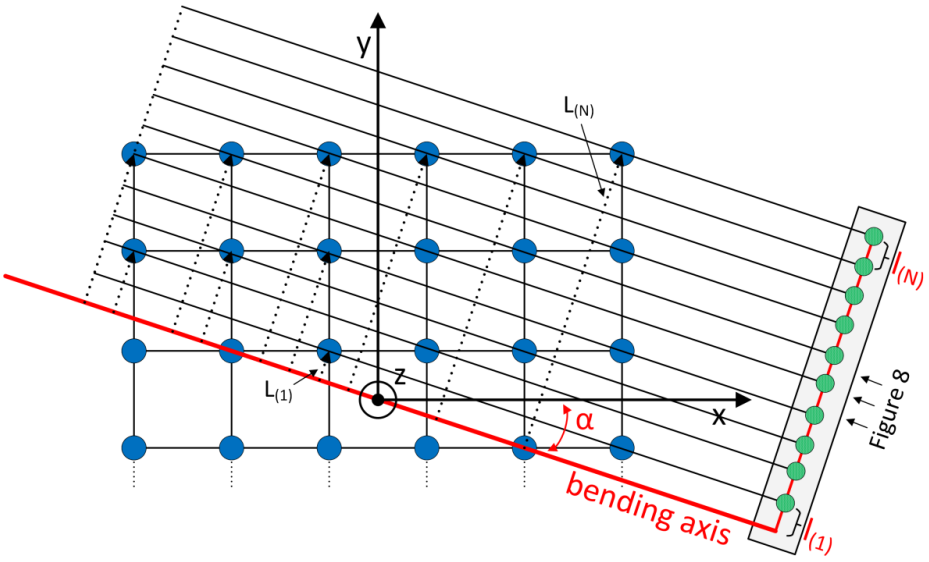

Figure 6: Division of the sensor array into discrete bending segments with the length $l_{(n)}$

The bending segments can be identified based on the shortest (perpendicular) distance $L_{S(ij)}(x, y, \alpha)$, between the bending axis and each sensor point as:

$$L_{S(ij)}(x, y, \alpha) = x * \sin(\alpha) + y * \cos(\alpha) \tag{3}$$

In the next step, $L_{S(ij)}$ with identical values are gathered whereby a monotonically increasing projection sequence is obtained as $L_{(1)}, \dots, L_{(N)}, (6 \leq N \leq 36)$, which allows us to calculate the length of each bending segment n as:

$$l_{(n)} = L_{(n)} - L_{(n-1)}, (n = 1 \dots N, \mathrm{L}_{(0)} = 0) \tag{4}$$

The bending radius $r_{(n)}$, in dependence of the measured output signal $V_{out}(\alpha, r)$, can be calculated via **Eq. 1** and **Eq 2** as:

$$r_{(n)} = V_{in} \cdot \frac{h}{V_{out}(\alpha,r)} \cdot \left[\frac{(1+q)}{2} + \frac{(1-q)}{2} \cdot cos(2\alpha)\right] \tag{5}$$

However, for sensor signals with orientations other than V_{s0}, the bending orientation angle α for **Eq. 6** has to be adapted as illustrated in **Figure 7.**

https://doi.org/10.24355/dbbs.084-201904011542-0

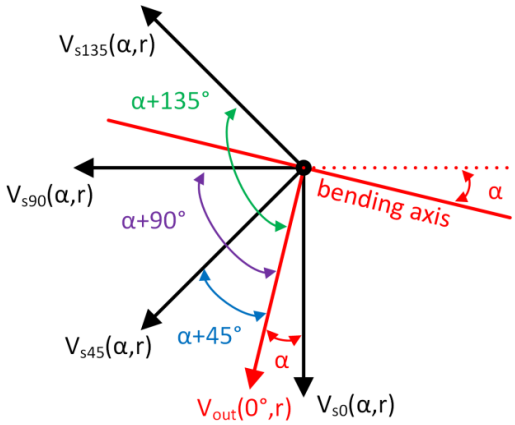

Figure 7: Sketch of sensor orientations relative to the bending angle α

Finally, we can introduce the surface reconstruction model on the basis of geometric relations between the parameters α, $l_{(n)}$ and $r_{(n)}$, as seen in **Figure 8**.

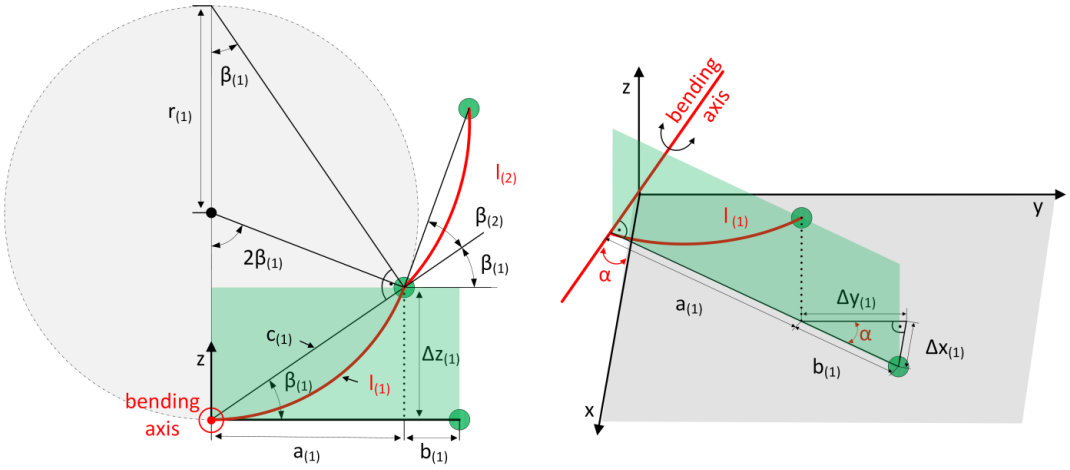

Figure 8: Schematic illustration of the surface reconstruction principle with appropriate geometrical definitions for calculating displacements of sensor notes in z-direction $\Delta z_{(n)}$ (left) and in x/y directions $\Delta x_{(n)}$, $\Delta y_{(n)}$ (right)

The bending induced displacements ($\Delta x_{(n)}, \Delta y_{(n)}, \Delta z_{(n)}$) for all sensors placed at distance $l_{(n)}$ from the bending axes can be calculated as:

$$\Delta x_{(n)} = b_{(n)} * sin(\alpha) \tag{6}$$

$$\Delta y_{(n)} = b_{(n)} * cos(\alpha) \tag{7}$$

$$\Delta z_{(n)} = c_{(n)} * sin\left(\sum_{n=1}^{N} \beta_{(n)}\right) \tag{8}$$

with help of the following geometrical relations, also displayed in **Figure 8**:

$$b_{(n)} = l_{(n)} - a_{(n)} \tag{9}$$

$$c_{(n)} = 2r_{(n)} * sin\left(\beta_{(n)}\right) \tag{10}$$

$$a_{(n)} = c_{(n)} * cos\left(\sum_{n=1}^{N} \beta_{(n)}\right) \tag{11}$$

$$2\beta_{(n)} = \frac{l_{(n)}}{r_{(n)}} \tag{12}$$

https://doi.org/10.24355/dbbs.084-201904011542-0

The transformation from S_{ij} in planar state to the final coordinates S'_{ij} in the bended foil can be described as:

$$S_{ij}(x_{ij}, y_{ij}, z_{ij}) \quad \text{->} \quad S'_{ij}\left(x_{ij} + \sum_{n=1}^{N} \Delta x_{(n)}\ , y_{ij} + \sum_{n=1}^{N} \Delta y_{(n)}\ , z_{ij} + \sum_{n=1}^{N} \Delta z_{(n)}\right)$$

using the previously made assignment of number pairs (i,j) with $(i = 1 \dots 6\,; j = 1 \dots 6)$ to numbers n $(n = 1 \dots N)$. The visualization of the reconstructed three-dimensional surface is obtained using the MATLAB function $\mathrm{surf}(x_{ij}, y_{ij}, z_{ij})$.

Even prior to the described surface reconstruction, we applied a sensor diagnosis to also handle rare cases of single dysfunctional sensors. For this aim, we distinguished between three kinds of sensor neighborhoods according to their position (sidewall, central and corner), as seen in **Figure 9,** and calculate a mean value V_m from the signals of a sensor and its neighbors. If the considered sensor signal exceeds the interval $0.7 * V_m - 1.3 * V_m$, it gets substituted by the mean value V_m. Although such kind of interpolation leads to a slight deviation from correct surface reconstruction, it prevents a failure of the complete system and renders it robust against failures of single sensors.

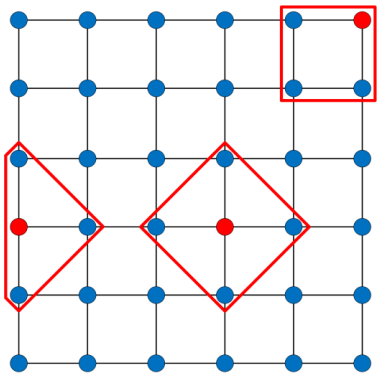

Figure 9: Definition of neighborhoods for three kinds of sensor positions (sidewall, central and corner)

An overview of the complete surface reconstruction process in the form of a flow chart is outlined in **Figure 10**.

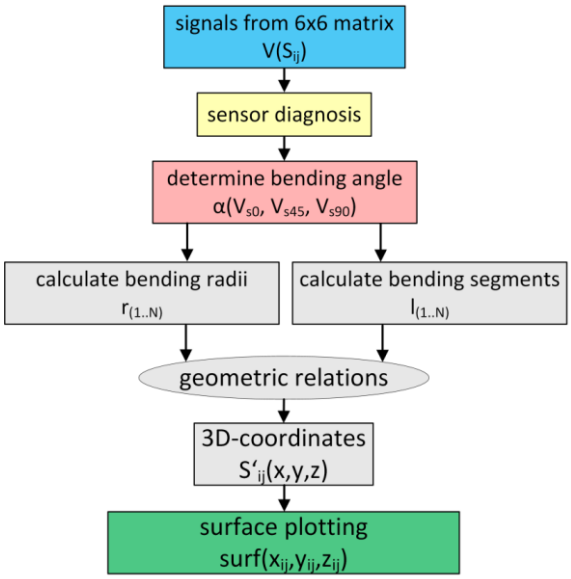

Figure 10: Flow chart presentation of the surface reconstruction process

https://doi.org/10.24355/dbbs.084-201904011542-0

4 Results and discussion

To demonstrate the functionality of the sensor foil array and the surface reconstruction method, we applied three different kinds of bending as illustrated in the photographs shown in **Figure 11 (left column).** Also, the raw sensor output signals **(middle column)** and the final surface reconstruction results **(right column)** are shown. The bending was applied by twisting the sensor foil over a glass test tube with a radius of 7.5 mm. The output signal was amplified 200 times.

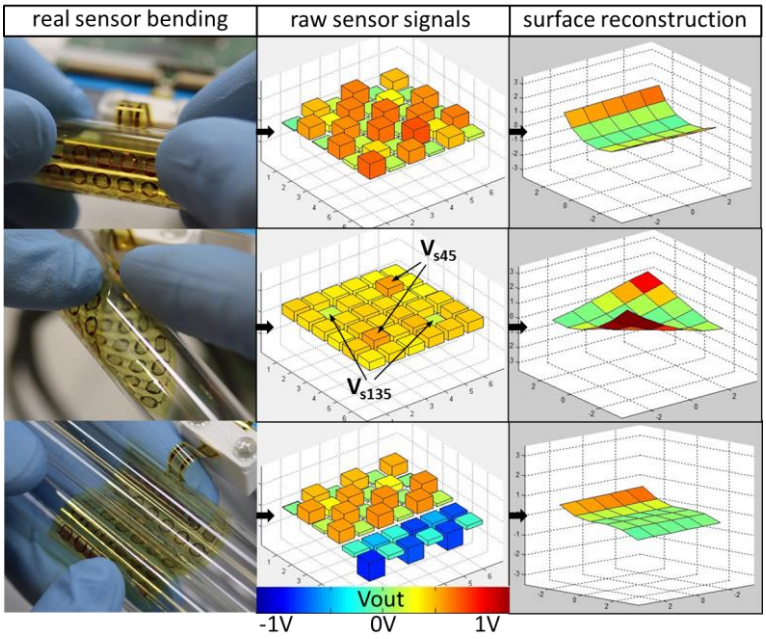

Figure 11: Results of surface reconstruction (right column) shown by bending the 6x6 sensor array (bending radius r=7.5mm) in three different modes (bending along sensor foil edge (top left), diagonal bending (middle left) and S-shape bending (bottom left)) with 3D bar chart representation of raw sensor signal (middle column).

Raw sensor signals clearly showed the dependence between sensor orientations according to **Figure 1b** and signal heights. For a bending axis parallel to the sensor foil edge, alternating heights of the raw sensor signals are evident in **Figure 11 (top row).** Diagonal bending provided almost identical output signals because vertically (s_0) and horizontally (s_{90}) orientated sensors received the same bending vector relative to their sensor axis **(middle row)**. Only the two diagonally orientated sensors s_{45} received a bending in the longitudinal direction and therefore provided a higher output signal. The two other diagonally orientated sensors s_{135} received a bending in transversal direction and accordingly showed a lower output signal. For the S-shaped bending, the switch in bending polarity between the two halves of the sensor array could be clearly seen by the switch in the signal sign from positive to negative values **(bottom row)**. The surface reconstruction results, as displayed in the **right column,** reflect the appropriate bending shapes seen in the **left column**. They are generated at a bending radius of 7.5 mm, providing high output signals. However, the higher the bending radius, the smaller the output signals, which in turn leads to more inaccurate surface reconstruction results. Smaller sensor signals are much more influenced by sensor noise, which was earlier determined to be +/- 10 mV (at 200x amplification)[9] . According to **Eq. 1,** this noise correlates to a variation in bending radius of +/− 759 mm. Sensor noise might be decreased by improving the electromagnetic compatibility of the sensor array (in example by covering the complete sensor array with a thin conductive shield layer). The sensor signal might be increased by increasing the interlayer thickness h (currently 11.5 µm) which, according to **Eq. 1,** has a direct influence on sensor sensitivity. A slightly thicker sensor foil would probably also be more shape-retaining and hence provide more precisely defined bending radii. A more stable detection of the bending orientation angle α could already be achieved by using mean values of multiple sensors for each of the required sensor signals V_{s0}, V_{s45}, V_{s90}. The diagnosis of dysfunctional sensors worked very well for isolated broken sensors with functioning neighboring ones. However, if more than two neighbored sensors are dysfunctional, the currently

https://doi.org/10.24355/dbbs.084-201904011542-0

applied sensor diagnosis and data repair is not sophisticated enough for accurate surface reconstruction and must be improved in future work.

5 Summary and outlook

A new method to reconstruct the surface of a flexible sensor array foil was introduced based on the signals of 6x6 integrated bending sensors and basic geometric relations in order to calculate the coordinates of each sensor after deformation. The current reconstruction algorithm was able to detect a single bending axis for the whole sensor foil by using plausibility considerations similar to the rules for resolving ambiguities as applied to strain gauge rosettes in structural health monitoring. The shown surface reconstruction results were largely in agreement with the applied bending shape, and the applied sensor diagnosis procedure was able to substitute signals of individual dysfunctional sensors with interpolated values. This guaranteed surface reconstruction even if single sensors did not work properly. With increasing bending radii, the surface reconstruction results became increasingly incorrect. This behavior is mainly influenced by sensor noise at low signal amplitudes which can be improved in future work by implementing electromagnetic shielding and increasing interlayer thickness. Future work with regard to the detection of more than one bending axis will allow more sophisticated surface reconstruction. Thus, the sensor array could, for example, be divided into four segments with potentially different bending axes, which would already allow independent determination of corner bends. A further segmentation would allow even more complex surface reconstruction, but would also need even more sophisticated reconstruction algorithms to patch the segments. A remedy could be provided by using different interpolation methods such as those already implemented in the MATLAB function “griddata”. The sensor design could also be improved by integrating two sensor elements of different orientations at one sensor node, which would allow a much more accurate detection of the bending angle. Careful evaluation of the surface reconstruction results and correlation with bending shape obtained by other means would be required for future work.

One of the potential applications is using the sensor foil as a respiratory monitoring tool by attaching it to the skin of a premature infant and measuring the foil bending induced by the body deformation between the thorax and abdomen [9]. Primarily, a trigger signal for the respiration device should be generated from the sensor signals. However, a surface reconstruction as addressed by this paper could also provide diagnostic information and help to further improve the medical treatment. This completely new information could be used, for example, to detect diseases like pneumothorax [11] which disables lung expansion. Another imaginable application could be found in structural health monitoring to measure the bending of various constructions.

Acknowledgements

The authors are grateful for the funding provided by the German Ministry of Economics and Technology (BMWi) under the ZIM program (Zentrales Innovationsprogramm Mittelstand) with the funding reference KF3085603TS4

6 References

[1] C. Rendl, M. Haller, S. Izadi, D. Kim, S. Fanello, P. Parzer, C. Rhemann, J. Taylor, M. Zirkl, G. Scheipl, T. Rothländer, FlexSense: A Transparent Self-Sensing Deformable Surface, in: the 27th annual ACM symposium, Honolulu, Hawaii, USA, pp. 129–138.

[2] A. Prochazka, O. Vysata, M. Schätz, H. Charvatova, Paz Suarez Araujo, Carmen, O. Geman, V. Marik, VIDEO PROCESSING AND 3D MODELLING OF CHEST MOVEMENT USING MS KINECT DEPTH SENSOR, in: 2016 International Workshop on Computational Intelligence for Multimedia Understanding (IWCIM), Reggio Calabria, Italy.

https://doi.org/10.24355/dbbs.084-201904011542-0

[3] J.-i. Watanabe, A. Mochizuki, Y. Horry, Bookisheet: Bendable Device for Browsing Content Using the Metaphor of Leafing Through the Pages, in: the 10th international conference, Seoul, Korea.
[4] S.-S. Lee, S. Maeng, D. Kim, K.-P. Lee, W. Lee, S. Kim, S. Jung, FlexRemote: Exploring the Effectiveness of Deformable User Interface as an Input Device for TV, in: C. Stephanidis (Ed.), HCI International 2011 – Posters' Extended Abstracts, Springer Berlin Heidelberg, Berlin, Heidelberg, 2011, pp. 62–65.
[5] R. Balakrishnan, G. Fitzmaurice, G. Kurtenbach, K. Singh, Exploring interactive curve and surface manipulation using a bend and twist sensitive input strip, in: the 1999 symposium, Atlanta, Georgia, United States, pp. 111–118.
[6] A. Dementyev, H.-L. Kao, J.A. Paradiso, SensorTape: Modular and Programmable 3D-Aware Dense Sensor Network on a Tape, in: the 28th Annual ACM Symposium, Daegu, Kyungpook, Republic of Korea, pp. 649–658.
[7] T. Consmüller, A. Rohlmann, D. Weinland, C. Druschel, G.N. Duda, W.R. Taylor, S. Milanese, Velocity of Lordosis Angle during Spinal Flexion and Extension, PLoS ONE 7 (2012) e50135.
[8] E. Szelitzky, A.-M. Aluţei, B. Chetran, D. Mândru, Data Glove and Virtual Environment - a Distance Monitoring and Rehabilitation Solution, in: E-Health and Bioengineering Conference (EHB), 2011, Iaşi, Romania.
[9] E. Koch, A. Dietzel, Skin attachable flexible sensor array for respiratory monitoring, Sensors and Actuators A: Physical 250 (2016) 138–144.
[10] Micro-Measurements, Strain Gage Rosettes: Selection, Application and Data Reduction: Tech Note TN-515, available at http://www.vishaypg.com/docs/11065/tn-515.pdf (accessed on April 14, 2016).
[11] D. Waisman, A. Landesberg, S. Kohn, A. Faingersh, I.C. Klotzman, A. Gover, I. Kessel, A. Rotschild, Chest dynamics asymmetry facilitates earlier detection of pneumothorax, J Perinatol 36 (2016) 157–159.

https://doi.org/10.24355/dbbs.084-201904011542-0